



# MBE growth of atomically smooth non-polar cubic AlN

T. Schupp\*, K. Lischka, D.J. As

Department of Physics, University of Paderborn, Warburger Str. 100, 33095 Paderborn, Germany

## ARTICLE INFO

### Article history:

Received 29 December 2009

Received in revised form

22 January 2010

Accepted 27 January 2010

Communicated by H. Asahi

Available online 4 February 2010

### Keywords:

A1. Atomic force microscopy

A1. Growth models

A1. High resolution X-ray diffraction

A1. Reflection high energy electron diffraction

A3. Molecular beam epitaxy

B1. Nitrides

## ABSTRACT

Atomically smooth cubic AlN (c-AlN) layers were grown by plasma assisted molecular beam epitaxy (PAMBE) using freestanding 3C-SiC substrates. A model based on reflection high electron energy diffraction (RHEED) transients has been developed to lead the way to optimal growth conditions. Confirmation of the cubic structure of the AlN layers was gained by high resolution X-ray diffraction (HRXRD) measurements yielding a lattice parameter of 4.373 Å. Finally atomic force microscopy (AFM) scans revealed an atomically smooth surface with a roughness of 0.2 nm RMS.

© 2010 Elsevier B.V. All rights reserved.

## 1. Introduction

The group-III nitrides AlN and GaN and their alloys are wide-bandgap semiconductors. They have a high chemical stability, a hardness comparable to sapphire, and a thermal conductivity comparable to copper. This set of properties makes them suitable for high power electronic and photonic devices. Current commercial group-III nitride-based electronic and optoelectronic devices are grown along the polar (0 0 1) *c*-direction of the crystal. This leads to piezoelectric and spontaneous polarization electrical fields. These fields change the behaviour of optoelectronic devices containing quantum wells (QW) or quantum dots (QD). The quantum confined stark effect induced by “built-in” electric fields leads to a reduced recombination probability of electrons and holes in the confined states. This longer radiative recombination time leads to less efficient and slower photonic devices. In contrast to the *c*-plane hexagonal phase, the metastable cubic phases of AlN (c-AlN) and GaN (c-GaN) have no polarization electrical fields in (0 0 1) growth direction [1]. Non-polar (0 0 1) oriented group-III nitride layers with zinc-blende structure and direct bandgap have shown higher recombination rates. For example, the radiative radiation time of cubic GaN QDs is 2 orders of magnitude below that of hexagonal *c*-plane GaN QDs [2].

For nanoscale devices the surface roughness is of great importance. High roughness can lead to broadening of confined electronic

states in low-dimensional structures and short circuits in electronic devices. Until now, cubic AlN has shown significant surface roughness and a tendency to form hexagonal inclusions [3].

We report on the PAMBE growth of atomically flat c-AlN layers with a surface roughness of 0.2 nm RMS. A growth procedure, which uses reflection high energy electron diffraction (RHEED) transients to control the growth front is developed to enable reproducible optimal growth conditions. Furthermore, we present a detailed HRXRD (1 1 3) reciprocal space map of the cubic AlN reflection and extract the lattice constant.

## 2. Experimental

The c-AlN layers were grown pseudomorphically strained on freestanding 3C-SiC (0 0 1) substrates by PAMBE. A Riber 32 growth chamber with Ga and Al Riber effusion cells was used. The nitrogen plasma was generated by an Oxford Instruments RF plasma source.

The substrates were cleaned with acetone, propanol, and buffer oxide etching in an ultrasonic bath. The final cleaning step of the substrate was performed in the MBE chamber by depositing and desorbing Al on the sample surface (Al flashes). The substrate temperature for Al flashes was 900 °C and Al flux was  $3 \times 10^{14} \text{ cm}^{-2} \text{ s}^{-1}$ . Before the initial growth of the c-AlN layer, one monolayer (ML) of Al was deposited on the surface. The growth began by simultaneously opening the Al and N shutters. The substrate temperature during c-AlN growth was 730 °C. The

\* Corresponding author. Tel.: +49 5251 60 5831; fax: +49 5251 60 5843.  
E-mail address: [schupp@post.com](mailto:schupp@post.com) (T. Schupp).

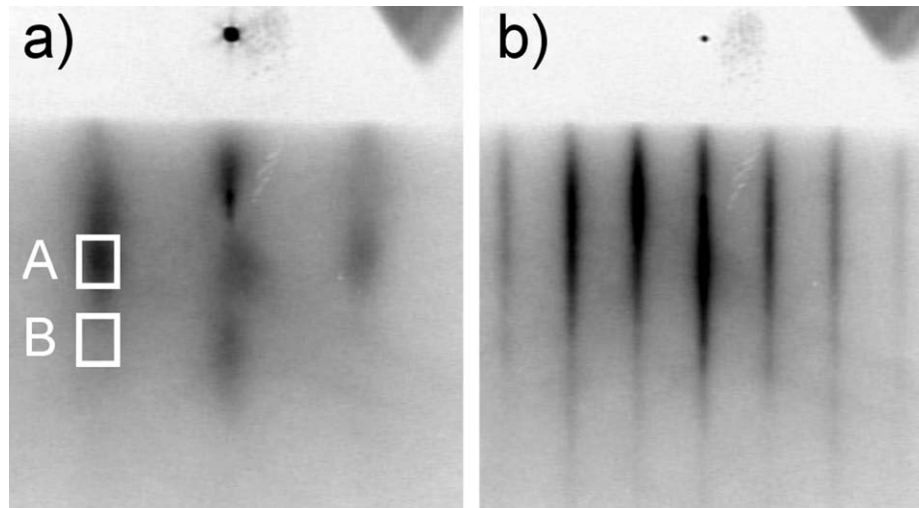


**Fig. 1.** RHEED patterns observed during the cleaning process of the 3C-SiC substrate with Al flashes. (a)  $[-1\ 1\ 0]$  azimuth of the 3C-SiC substrate before Al flashes, and (b)  $[-1\ 1\ 0]$  azimuth of the 3C-SiC substrate after Al flashes.

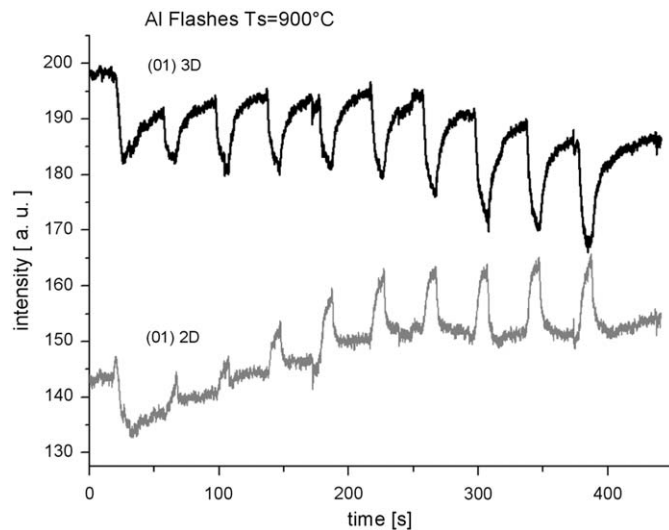


**Fig. 2.** Intensity of two different spots in the RHEED pattern of the 3C-SiC surface during the repeated deposition and desorption of Al.

growth rate of 150 nm/h was determined by the RHEED specular spot intensity oscillations (RHEED oscillations).

### 3. Results and discussion

#### 3.1. Deoxidation

The surface preparation is of great importance for an epitaxial growth process such as MBE, because any disturbances on the surface can lead to crystal defects in the grown layer. Fig. 1(a) shows the RHEED pattern of the 3C-SiC (001) surface in  $[-1\ 1\ 0]$  azimuth before deoxidation. Amorphous surface oxides like  $\text{SiO}_2$  cause blurred reflections in the RHEED pattern of the cubic lattice. The elliptical shape of reflections is due to an electron transmission component through 3D islands on the surface [4]. By distinguishing the electron reflection and electron transmission component in the RHEED image the transition of the surface can be observed. The graphs in Fig. 2 show the intensity versus time behaviour of two spots in the substrate RHEED pattern during the repeated deposition and desorption of Al layers. The black graph shows the intensity of a

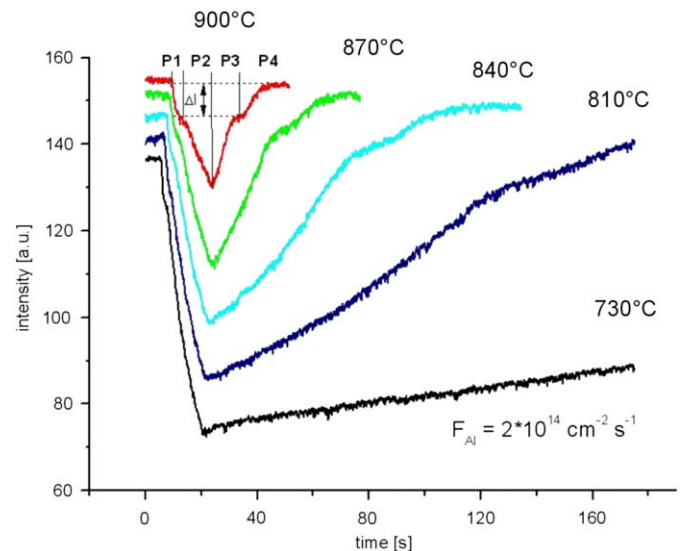


**Fig. 3.** Intensity of the (01) RHEED reflection of the c-AlN surface during the deposition and desorption of Al. The substrate temperature is varied between 730 and 900 °C.

RHEED pattern area associated with the 3D islands on the surface, marked as letter A in Fig. 1. The grey graph shows the intensity of a RHEED pattern area associated with the 2D part of the surface, marked as letter B in Fig. 1. The average intensity of the black graph decreases with each Al flash cycle, whereas the average intensity of the grey graph increases. This behaviour is associated with the reduction in 3D oxide islands. The cycle amplitude of both graphs increases with each flash, indicating an increase in the surface sensitivity. After the deoxidation procedure, the RHEED pattern of 3C-SiC surface in Fig. 1(b) shows long thin streaks with a  $(2 \times 4)$  reconstruction. The reduction in FWHM of the intensity profile of the cubic reflections indicates the removal of amorphous oxides from the surface. The absence of spotty reflections shows that the 3D islands have vanished.

#### 3.2. Al surface kinetics

Due to the metastable nature of cubic AlN, exposing a c-AlN surface to nitrogen favours the formation of hexagonal clusters.

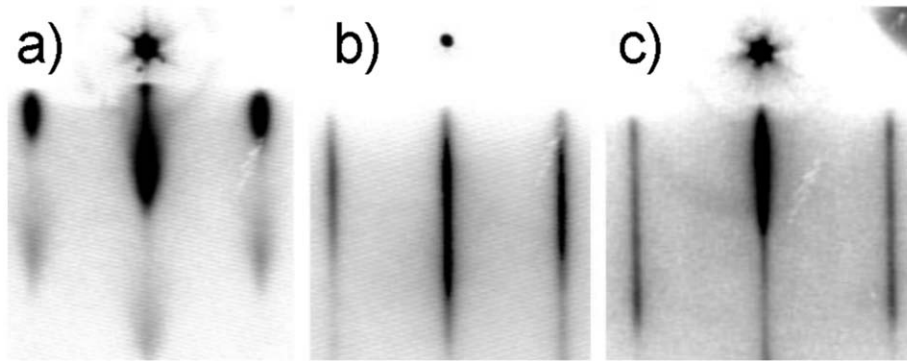


Fig. 4. RHEED patterns of the c-AlN surface during the initial growth process. (a) after growth of 6 ML, (b) after growth of 30 ML, and (c) after growth of 650 ML

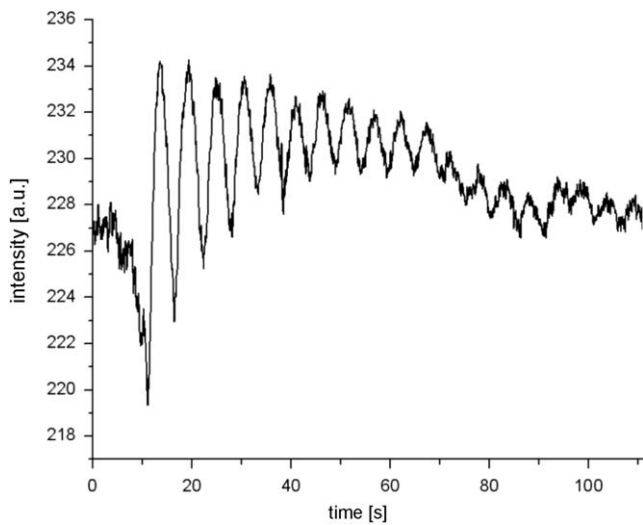


Fig. 5. RHEED specular spot intensity vs. time. Each oscillation indicates the growth of one atomic layer of c-AlN.

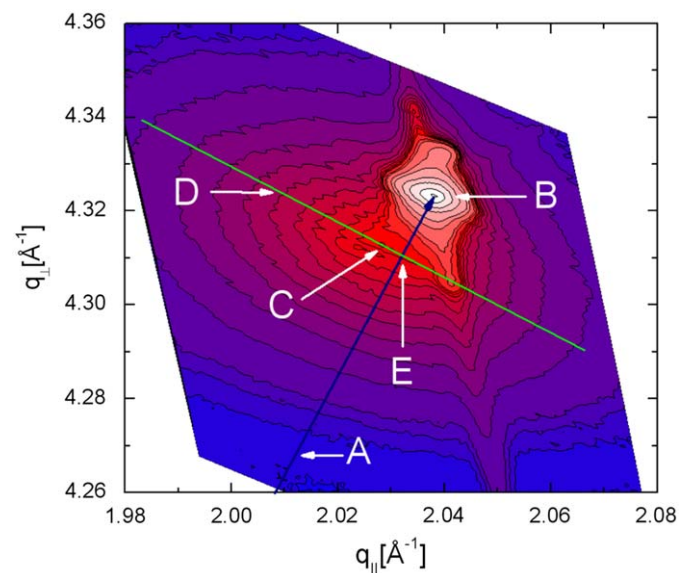


Fig. 6. HRXRD reciprocal space map of the (1 1 3) reflections of c-AlN and 3C-SiC. (A) reciprocal lattice vector of 3C-SiC reflection, (B) 3C-SiC reflection, (C) position of the c-AlN peak, (D) axis for tilt correction perpendicular to A, and (E) position of c-AlN peak after tilt correction.

Growth under one monolayer Al surface coverage can prevent hexagonal condensation. To reliably maintain one ML Al surface coverage, a model linking RHEED reflection intensity with Al surface coverage has been developed. This model is based on a model originally designed for Ga surface coverage on a c-GaN surface introduced by Schörmann et al [5]. One key element of the model is the difference in the RHEED reflection intensity between a c-AlN surface and an Al surface. The graphs in Fig. 3 display the intensity change over time of the RHEED (0 1) reflection at various surface temperatures. Al is deposited on and desorbed off a c-AlN layer with a temperature between 730 and 900 °C. The graphs show two distinct kinks  $\Delta I$  below the maximum intensity. One kink can be observed during Al adsorption and the other during Al desorption. We associate the intensity change between the maximum intensity and the aforementioned kinks with one monolayer of Al coverage on a c-AlN surface. As shown in Fig. 3, the Al surface coverage model consists of 4 phases. Phase 1 is linked with the adsorption of the first monolayer of Al on the c-AlN surface. It begins at zero Al coverage and ends at one monolayer. Phase 2 is associated with the formation of Al droplets on the surface leading to further intensity decrease due to electron scattering. Phase 3 is linked to the desorption of Al droplets. During this phase there is also desorption from the entire Al monolayer. The adhesion force between Al atoms and the c-AlN surface is higher than the cohesion force between the Al atoms. The droplets act as reservoirs of Al, feeding the monolayer and stabilizing the one monolayer coverage. Although the

desorption rate varies for different surface temperatures, the intensity difference  $\Delta I$  between kink and maximum intensity is the same. This is further confirmation for the connection between Al surface coverage and RHEED intensity.

Phase 4 is associated with the desorption of the Al monolayer.

### 3.3. Growth of cubic AlN

The first step in the growth process is the deposition of one monolayer of Al on the substrate surface. The c-AlN condensation starts by simultaneously opening the Al and N shutters. A comparison between the RHEED pattern of the substrate in Fig. 1(b) with the RHEED pattern after the deposition of 6 ML of c-AlN in Fig. 4(a) reveals a transition from 2D to 3D surface. This transition can be inferred from the transformation of the long streaks into spotty reflections. These reflections originate from an electron transmission component through islands on the surface. The formation of c-AlN islands is driven by the difference in the surface energy of 3C-SiC and c-AlN. Right at the beginning of the growth, when the first c-AlN clusters are formed, both materials share one surface. 3C-SiC has a lower surface energy than c-AlN; so it is energetically favourable to maintain a maximum of 3C-SiC

surface area and only a minimum of c-AlN surface area. This is achieved by the formation of c-AlN islands. After the growth of 10–20 monolayers of c-AlN, a roughness transition is observed. The surface transforms into an atomically smooth 2D state. This can be concluded from the RHEED pattern of the c-AlN surface in Fig. 4(b). The spotty reflections are replaced by long thin streaks. The surface transition to a 2D state can be explained by surface energy as well. When the entire 3C-SiC surface is overgrown with c-AlN, the influence of 3C-SiC diminishes. Since the area of a surface covered with islands is larger than that of a flat 2D surface, the 2D surface has a lower total surface energy. Thus, the formation of a 2D c-AlN surface is energetically favourable.

However, the transformation from the 3D to the 2D state depends also on the Al coverage of the growth front. For a N-terminated surface, the migration of Al-adsorbates is realized via strong covalent Al–N bonds. These bonds reduce the Al surface diffusion length significantly. This leads to 3D Volmer–Weber growth, increased surface roughness, and eventually hexagonal condensation. For an Al covered surface this behaviour is different. The Al monolayer may be considered as liquid phase where the Al adsorbate migration is predominantly realized via delocalized weak Al–Al bonds. Thus, for an Al terminated surface, the diffusion barrier of Al adatoms is significantly lower than the diffusion barrier of N adatoms. Consequently, the low diffusion barrier results in a high Al surface diffusion length allowing Frank–Van der Merwe layer by layer growth [6].

The initial growth is completed after 30 monolayers of c-AlN. The growth is continued in cycles of 20 atomic layers with growth interruptions of 30 s afterwards. These interruptions allow the

surface adatoms to fill distant vacancies by surface migration. One indication for vacancies is the dampening of RHEED oscillations as shown in Fig. 5. The amount of RHEED oscillations correlates with the perfection of the layer by layer growth. With sufficient long growth interruptions, the surface quality can be recovered and layer-by-layer growth can be re-established. The c-AlN thickness was controlled by RHEED oscillations yielding a growth rate of 0.2 ML/s. After the growth of 650 ML c-AlN, the RHEED pattern in Fig. 4(c) still indicates a smooth 2D surface. Under optimal growth conditions, the main RHEED azimuths show patterns of the cubic lattice; hexagonal reflections are absent.

### 3.4. High resolution X-ray diffraction

The cubic structure of the AlN layer is verified by HRXRD measurements. Fig. 6 shows the HRXRD (1 1 3) reciprocal space map of a 300 nm c-AlN layer on 3C-SiC. Arrow A indicates the (1 1 3) 3C-SiC reciprocal lattice vector. Arrow B indicates the position of the 3C-SiC Bragg peak. Arrow C indicates the position of the c-AlN reflection. The elliptic shape originates from a mosaic structure and is caused by strain relaxation [7]. The main axis of the ellipse (arrow D in Fig. 6) is perpendicular to the reciprocal lattice vector. A small shift in the c-AlN peak along the main axis can be interpreted as tilt of the c-AlN layer versus the substrate. Taking into account this tilt, the position of the c-AlN reflection is located at arrow E in Fig. 6. The cubic AlN lattice constant extracted from Fig. 6 is  $4.373 \text{ \AA} + 0.002 \text{ \AA}$ . This is in good agreement with a calculation based on the hexagonal lattice

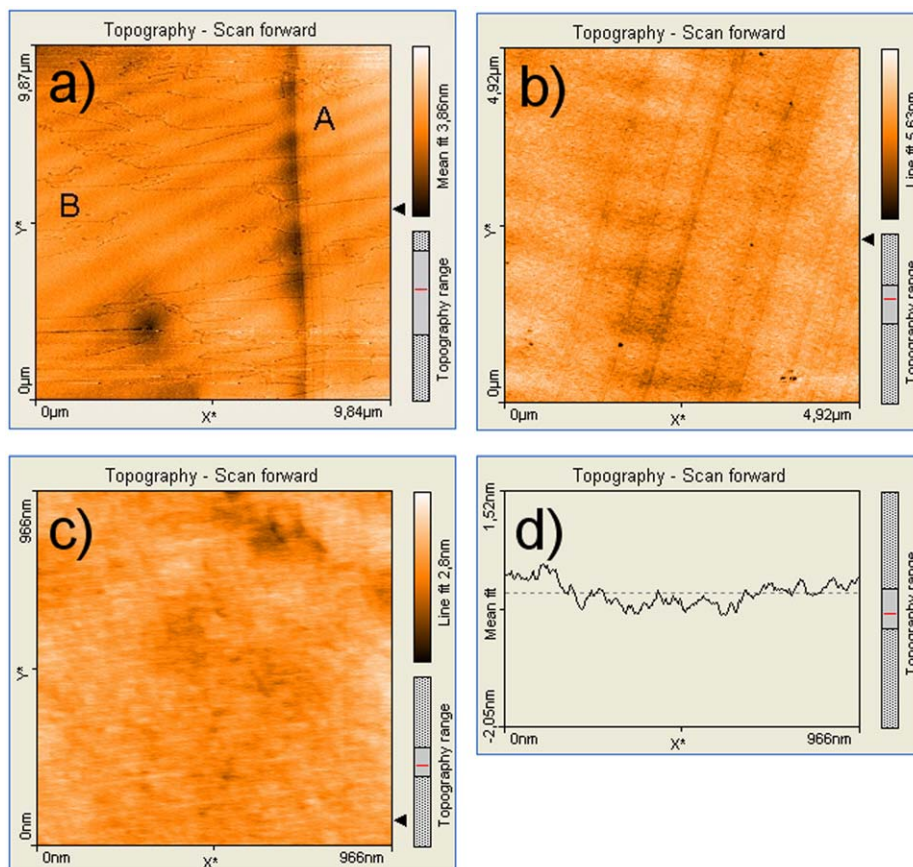


**Fig. 7.** AFM images: (a)  $10 \times 10 \mu\text{m}^2$  area of the 3C-SiC substrate, (b)  $5 \times 5 \mu\text{m}^2$  area of the 150 nm thick c-AlN layer, (c)  $1 \times 1 \mu\text{m}^2$  area of the c-AlN layer with a roughness of 0.2 nm RMS, and (d) line scan of (c).

parameters, where we assume equal bond length in the cubic and hexagonal lattice (Eq. (1)) resulting in a cubic lattice constant of 4.37 Å [8].

$$a_{\text{cubic}} = \sqrt[3]{\sqrt{3} \times a_{\text{hex}} \times c_{\text{hex}}} = \sqrt[3]{\sqrt{3} \times 3.11 \times 4.98} = 4.37 \text{ \AA} \quad (1)$$

The FWHM of the intensity along the main axis of the ellipse of the c-AlN (1 1 3) reflection is 29 arc min. This is comparable with the FWHM of the (0 0 2) rocking curve. The FWHM may be transferred into a dislocation density of the c-AlN layer. Using the relation given in Ref. [9] we obtain a dislocation density in our layers of about  $8 \times 10^9 \text{ cm}^{-2}$ .

### 3.5. Atomic force microscopy

The surface quality of our samples were analyzed by AFM measurements. Fig. 7(a) shows a  $10 \times 10 \mu\text{m}^2$  area of the 3C-SiC substrate surface. Close to region A, parallel lines originating from anti-boundary defects can be identified. Secondly, line defects associated with surface oxides can be seen close to B. The third effect is a wave pattern over the entire surface. This pattern is a known AFM artifact measured on smooth surfaces [10]. The surface roughness of the substrate including boundary defects is 1 and 0.5 nm without the defects. Fig. 7(b) shows a  $5 \times 5 \mu\text{m}^2$  area of the c-AlN surface with parallel lines originating from anti-boundary defects. Including the anti-boundary defects, the surface roughness is 0.6 nm RMS. The wave pattern due to an AFM artefact is also present in this image. A  $1 \times 1 \mu\text{m}^2$  area of the c-AlN surface without anti-boundary defects is shown in Fig. 7(c). Here the surface roughness is only 0.2 nm RMS. The line scan of Fig. 7(d) depicts a peak-to-valley height of 1 lattice constant over a lateral extension of  $\sim 2000$  lattice constants, validating the atomically smooth surface.

## 4. Conclusion

Atomically smooth c-AlN layers on 3C-SiC substrates have been grown by PAMBE. Measurements of the RHEED transients enabled the growth under 1 monolayer of Al coverage, preventing hexagonal AlN inclusions. AFM scans and RHEED patterns verified the atomically flat surface. The HRXRD measurements confirmed the cubic structure of the AlN layers and yield a lattice parameter of 4.373 Å.

## Acknowledgements

This work was supported by the DFG graduate program GRK 1464 "Micro- and Nanostructures in Optoelectronics and Photonics". We would like to thank Dr. M. Abe and Dr. H. Nagasawa at HOYA Corporation for the supply of the 3C-SiC substrates.

## References

- [1] D.J. As, *Microelectron. J.* 40 (2009) 204.
- [2] J. Simon, N.T. Pelekanos, C. Adelman, E. Martinez-Guerrero, R. André, B. Daudin, Le Si Dang, H. Mariette, *Phys. Rev. B* 68 (2003) 035312.
- [3] V. Lebedev, V. Cimalla, U. Kaiser, Ch. Foerster, J. Pezoldt, J. Biskupek, O. Ambacher, *J. Appl. Phys.* 97 (2005) 114306.
- [4] W. Braun, *Applied RHEED*, Springer Tracts in Modern Physics, Vol. 154, Springer, Berlin, 1999.
- [5] J. Schörmann, S. Potthast, D.J. As, K. Lischka, *Appl. Phys. Lett.* 90 (2007) 041918.
- [6] T. Zywietz, J. Neugebauer, M. Scheffler, *Appl. Phys. Lett.* 73 (1998) 487.
- [7] V. Holy, *High-resolution X-ray scattering from thin films and multilayers*, Springer Tracts in Modern Physics, Vol. 149, Springer, Berlin, 1999.
- [8] D.J. As, *Optoelectronic Properties of Semiconductors and Superlattices*, Vol. 19, Taylor & Francis, New York, 2003.
- [9] P. Gay, P.B. Hirsch, A. Kelly, *Acta Metall.* 1 (1953) 315.
- [10] A. Mendez-Vilas, M.L. Gonzalez-Martín, L. Labajos-Broncano, M.J. Nuevo, *Appl. Surf. Sci.* 238 (2004) 42.